IOPscience iopscience.iop.org

Home Search Collections Journals About Contact us My IOPscience

# New $Mo_2FeB_2$ type intermetallic cadmium compounds $RE_2Pd_2Cd$ (RE = Pr, Sm, Gd–Lu)—synthesis, structure, and magnetic properties

This article has been downloaded from IOPscience. Please scroll down to see the full text article.

2007 J. Phys.: Condens. Matter 19 026209

(http://iopscience.iop.org/0953-8984/19/2/026209)

View the table of contents for this issue, or go to the journal homepage for more

Download details:
IP Address: 129.252.86.83
The article was downloaded on 28/05/2010 at 15:20

Please note that terms and conditions apply.

INSTITUTE OF PHYSICS PUBLISHING JOURNAL OF PHYSICS: CONDENSED MATTER

J. Phys.: Condens. Matter **19** (2007) 026209 (17pp) doi:10.1088/0953-8984/19/2/026209

# New $Mo_2FeB_2$ type intermetallic cadmium compounds $RE_2Pd_2Cd$ (RE = Pr, Sm, Gd–Lu)—synthesis, structure, and magnetic properties

**Ahmet Doğan, Sudhindra Rayaprol and Rainer Pöttgen**

Institut für Anorganische und Analytische Chemie, Westfälische Wilhelms-Universität Münster, Corrensstraße 30, 48149 Münster, Germany

E-mail: pottgen@uni-muenster.de

Received 11 October 2006, in final form 9 November 2006
Published 15 December 2006
Online at stacks.iop.org/JPhysCM/19/026209

**Abstract**

The intermetallic cadmium compounds $RE_2Pd_2Cd$ (RE = Pr, Sm, Gd–Lu) were synthesized by induction-melting of the elements in sealed tantalum tubes. The samples were characterized through x-ray powder patterns. The structures of $RE_2Pd_2Cd$ (RE = Pr, Sm, Gd, Dy, Yb) were refined on the basis of x-ray single-crystal data: $Mo_2FeB_2$ type, $P4/mbm$, $a = 774.92(9)$, $c = 389.3(1)$ pm, $wR2 = 0.0756$, 215 $F^2$ values for $Pr_2Pd_2Cd$, $a = 769.34(9)$, $c = 381.46(8)$ pm, $wR2 = 0.0357$, 307 $F^2$ values for $Sm_2Pd_2Cd$, $a = 766.50(8)$, $c = 376.57(5)$ pm, $wR2 = 0.0363$, 202 $F^2$ values for $Gd_2Pd_2Cd$, $a = 763.8(1)$, $c = 370.81(8)$ pm, $wR2 = 0.0581$, 191 $F^2$ values for $Dy_2Pd_2Cd$, $a = 757.5(2)$, $c = 371.6(1)$ pm, $wR2 = 0.0448$, 284 $F^2$ values for $Yb_2Pd_2Cd$ with 12 variables per refinement. The $RE_2Pd_2Cd$ compounds are intergrowths of distorted $AlB_2$ and CsCl related slabs of compositions $REPd_2$ and RECd. Magnetic ordering was observed in the compounds of the series $RE_2Pd_2Cd$ (with RE = Pr, Sm, Gd, Tb, Dy, and Er). $Pr_2Pd_2Cd$ and $Dy_2Pd_2Cd$ undergo ferromagnetic ordering at 11 and 20 K, whereas $Gd_2Pd_2Cd$, $Tb_2Pd_2Cd$, and $Er_2Pd_2Cd$ order antiferromagnetically at 56, 55, and 12 K respectively. $Sm_2Pd_2Cd$ exhibits van Vleck paramagnetism. The results of crystallographic investigations along with magnetic measurements and specific heat studies are presented and discussed herein.

## 1. Introduction

The intermetallic compounds $RE_2T_2X$ (RE = rare earth metal, T = transition metal, and X = In, Sn, Mg, Cd) with $Mo_2FeB_2$ and $Er_2Au_2Sn$ type structure have been thoroughly studied in recent years with respect to their unusual magnetic and electrical properties [1]. While the indides and stannides of these series have widely been investigated, only a little information is

available on corresponding magnesium and cadmium based materials, mainly due to problems in sample preparation. The indides and stannides can easily be prepared via arc-melting. Due to the comparatively low boiling temperatures of magnesium (1363 K) and cadmium (1038 K) [2], synthesis in a quasi-open system would result in significant evaporations. The $RE_2T_2Mg$ and $RE_2T_2Cd$ compounds therefore need to be prepared in sealed, high-melting metal tubes (niobium or tantalum) [3].

With cadmium, so far, the series $RE_2Ni_2Cd$ (RE = La, Ce, Pr, Nd, Sm, Tb, Dy) [4, 5], $RE_2Rh_2Cd$ (RE = La, Ce, Pr, Nd, Sm) [6], $RE_2Pd_2Cd$ (RE = La, Ce, Nd) [3, 7], $Ce_2Pt_2Cd$ [3], and $RE_2Au_2Cd$ (RE = La, Ce, Pr, Nd, Sm, Gd) [8–10] have been reported. The course of the cell parameters indicated intermediate cerium valence for $Ce_2Ni_{1.88}Cd$ [4] and $Ce_2Rh_{1.86}Cd$ [6], as was also evident from susceptibility data for $Ce_2Ni_{1.88}Cd$ [4]. In contrast, $Ce_2Au_2Cd$ [9] contains trivalent cerium and can be considered as a heavy fermion system with antiferromagnetic ordering around 5 K. $Gd_2Au_2Cd$ exhibits coexistence of ferromagnetism and spin-glass anomalies [10].

Recently we reported on the magnetic and heat capacity data of $RE_2Pd_2Cd$ (RE = La, Ce, Nd) [7]. Within this series $La_2Pd_2Cd$ is a Pauli paramagnet, $Ce_2Pd_2Cd$ is a 5 K antiferromagnet with Kondo interactions and $Nd_2Pd_2Cd$ orders ferromagnetically at $T_C$ = 23.7 K. In continuation to our investigations on $RE_2T_2Cd$ intermetallics we present here the structural, magnetic, and heat capacity data of $RE_2Pd_2Cd$ for RE = Pr, Sm, and Gd–Lu.

## 2. Experimental details

The starting materials for the preparation of the $RE_2Pd_2Cd$ compounds were ingots of the rare earth elements (Johnson-Matthey or Kelpin), palladium powder (about 200 mesh, Degussa-Hüls), and a cadmium rod (Johnson-Matthey), all with a stated purity better than 99.9%. The rare earth metal ingots were cut into smaller pieces and arc-melted into small buttons under purified argon. The elements were then weighed in 2:2:1 atomic ratio and sealed in small tantalum tubes under purified argon [11]. The tantalum tubes were then placed in a water-cooled quartz sample chamber of a high frequency furnace (Hüttinger Elektronik, Freiburg, type TIG 1.5/300) under flowing argon [12] and first heated at 1670 K for about one minute followed by annealing at around 870 K for 2–4 hours. The temperature was controlled through a Sensor Therm Methis MS09 pyrometer with an accuracy of ±30 K. The synthesis conditions are similar to those given in [3].

The samples were characterized through Guinier powder patterns using Cu K$\alpha_1$ radiation and $\alpha$-quartz ($a$ = 491.30, $c$ = 540.46 pm) as an internal standard. The lattice parameters (table 1) were deduced from least squares refinements of the Guinier data. To ensure correct indexing, the experimental patterns were compared to calculated ones [13] taking the atomic positions of the structure refinements. The powder and single crystal lattice parameters agreed well.

Irregularly shaped single crystals of $Pr_2Pd_2Cd$, $Sm_2Pd_2Cd$, $Gd_2Pd_2Cd$, $Dy_2Pd_2Cd$, and $Yb_2Pd_2Cd$ were isolated from the samples by mechanical fragmentation. They were examined by Laue photographs on a Buerger precession camera (equipped with a Fujifilm BAS-1800 imaging plate system) in order to establish suitability for intensity data collection. Intensity data of the $Pr_2Pd_2Cd$, $Sm_2Pd_2Cd$ and $Yb_2Pd_2Cd$ crystals were collected at room temperature on a four-circle diffractometer (CAD4) with graphite monochromatized Mo K$\alpha$ radiation (71.073 pm) and a scintillation counter with pulse height discrimination. The scans were performed in the $\omega/2\theta$ mode. Empirical absorption corrections were applied on the basis of $\Psi$-scan data followed by spherical absorption corrections. Intensity data of $Gd_2Pd_2Cd$ and $Dy_2Pd_2Cd$ were collected in oscillation mode on a Stoe IPDS-II image plate diffractometer

**Table 1.** Lattice parameters of the tetragonal intermetallic cadmium compounds $RE_2Pd_2Cd$.

| Compound | $a$ (pm) | $c$ (pm) | $V$ (nm$^3$) | Reference |
|---|---|---|---|---|
| $La_2Pd_2Cd$ | 784.47(8) | 398.03(9) | 0.2449 | This work |
| $Ce_2Pd_2Cd$ | 777.90(6) | 393.28(6) | 0.2380 | [3] |
| $Ce_2Pd_2Cd$ | 778.3(1) | 392.9(2) | 0.2380 | This work |
| $Pr_2Pd_2Cd$ | 774.92(9) | 389.3(1) | 0.2338 | This work |
| $Nd_2Pd_2Cd$ | 774.15(9) | 386.73(7) | 0.2318 | [7] |
| $Sm_2Pd_2Cd$ | 769.34(9) | 381.46(8) | 0.2258 | This work |
| $Gd_2Pd_2Cd$ | 766.50(8) | 376.57(5) | 0.2212 | This work |
| $Tb_2Pd_2Cd$ | 765.96(8) | 373.69(7) | 0.2192 | This work |
| $Dy_2Pd_2Cd$ | 763.8(1) | 370.81(8) | 0.2163 | This work |
| $Ho_2Pd_2Cd$ | 763.80(8) | 367.50(8) | 0.2144 | This work |
| $Er_2Pd_2Cd$ | 763.1(1) | 365.84(8) | 0.2130 | This work |
| $Tm_2Pd_2Cd$ | 760.43(7) | 362.98(8) | 0.2099 | This work |
| $Yb_2Pd_2Cd$ | 756.4(1) | 371.5(1) | 0.2126 | [15] |
| $Yb_2Pd_2Cd$ | 757.5(2) | 371.6(1) | 0.2132 | This work |
| $Lu_2Pd_2Cd$ | 760.8(1) | 359.6(1) | 0.2081 | This work |

using monochromatized Mo K$\alpha$ radiation (71.073 pm). Numerical absorption corrections were applied to these data sets. All relevant crystallographic details are listed in table 2.

All data sets were compatible with space group $P4/mbm$. The atomic parameters of $Nd_2Pd_2Cd$ [7] were taken as starting values and the structures were refined using SHELXL-97 (full-matrix least-squares on $F_o^2$) [14] with anisotropic atomic displacement parameters for all sites. As a check for the correct compositions, the occupancy parameters were refined in separate series of least-squares cycles. All sites were fully occupied within two standard uncertainties and in the final cycles the ideal occupancies were assumed again. Final difference Fourier syntheses revealed no significant residual peaks (table 2). The refined positional parameters and interatomic distances (exemplary for $Gd_2Pd_2Cd$) are listed in tables 3 and 4. Further details on the structure refinements are available[1].

All bulk samples and the single crystals measured on the diffractometers were analysed in a Leica 420i scanning electron microscope via EDX. The rare earth trifluorides, palladium, and cadmium were used as standards. No impurity elements heavier than sodium (detection limit of the machine) were detected. The experimentally determined compositions were very close to the ideal ones. The EDX analyses gave no hint of homogeneity ranges.

Magnetism and heat capacity of $RE_2Pd_2Cd$ (RE = Pr, Sm, Gd, Tb, Dy, and Er) were measured on a Quantum Design physical property measurement system using ACMS (only for $Pr_2Pd_2Cd$), VSM, and HC options, respectively.

## 3. Results and discussion

### *3.1. Crystal chemistry*

The $RE_2Pd_2Cd$ compounds adopt the tetragonal $Mo_2FeB_2$ type structure, space group $P4/mbm$. As an example we present a projection of the $Gd_2Pd_2Cd$ structure onto the $xy$ plane in figure 1. The $Gd_2Pd_2Cd$ structure can be considered as a 1:1 intergrowth of $AlB_2$ and CsCl related slabs of compositions $GdPd_2$ and GdCd. As expected from the lanthanoid

[1] Details may be obtained from Fachinformationszentrum Karlsruhe, D-76344 Eggenstein-Leopoldshafen (Germany), by quoting the registry nos CSD-417014 ($Pr_2Pd_2Cd$), CSD-417015 ($Sm_2Pd_2Cd$), CSD-417016 ($Gd_2Pd_2Cd$), CSD-417018 ($Dy_2Pd_2Cd$), and CSD-417017 ($Yb_2Pd_2Cd$).

**Table 2.** Crystal data and structure refinements for $RE_2Pd_2Cd$ (RE = Pr, Sm, Gd, Dy, Yb), $Mo_2FeB_2$ type, space group $P4/mbm$, Pearson symbol tP10, $Z = 2$.

| Empirical formula | $Pr_2Pd_2Cd$ | $Sm_2Pd_2Cd$ | $Gd_2Pd_2Cd$ | $Dy_2Pd_2Cd$ | $Yb_2Pd_2Cd$ |
|---|---|---|---|---|---|
| Molar mass | 607.02 g mol$^{-1}$ | 625.90 g mol$^{-1}$ | 639.70 g mol$^{-1}$ | 650.20 g mol$^{-1}$ | 671.28 g mol$^{-1}$ |
| Unit cell dimensions | Table 1 | Table 1 | Table 1 | Table 1 | Table 1 |
| Calculated density | 8.62 g cm$^{-3}$ | 9.21 g cm$^{-3}$ | 9.60 g cm$^{-3}$ | 9.98 g cm$^{-3}$ | 10.46 g cm$^{-3}$ |
| Crystal size | $40 \times 40 \times 140$ $\mu$m$^3$ | $20 \times 20 \times 160$ $\mu$m$^3$ | $20 \times 20 \times 110$ $\mu$m$^3$ | $80 \times 80 \times 120$ $\mu$m$^3$ | $10 \times 10 \times 200$ $\mu$m$^3$ |
| Detector distance | — | — | 60 mm | 60 mm | — |
| Exposure time | — | — | 5 min | 5 min | — |
| $\omega$ range; increment | — | — | 0°–180°, 1.0° | 0°–180°, 1.0° | — |
| Integr. param. $A$, $B$, EMS | — | — | 13.5, 3.5, 0.014 | 14.0, 4.0, 0.025 | — |
| Transm. ratio (max/min) | 1.67 | 1.97 | 1.26 | 3.39 | 1.65 |
| Absorption coefficient | 32.3 mm$^{-1}$ | 37.8 mm$^{-1}$ | 42.0 mm$^{-1}$ | 46.9 mm$^{-1}$ | 56.4 mm$^{-1}$ |
| F(000) | 516 | 528 | 536 | 544 | 560 |
| $\theta$ range | 3°–30° | 3°–35° | 3°–30° | 3°–30° | 3°–35° |
| Range in $hkl$ | $\pm10$, $\pm10$, $+5$ | $\pm12$, $\pm12$, $\pm6$ | $\pm10$, $\pm10$, $\pm5$ | $\pm10$, $\pm10$, $\pm5$ | $\pm12$, $\pm12$, $\pm5$ |
| Total no of reflections | 1449 | 3780 | 2118 | 2091 | 3480 |
| Independent reflections | 215 ($R_{int} = 0.113$) | 307 ($R_{int} = 0.027$) | 202 ($R_{int} = 0.052$) | 191 ($R_{int} = 0.029$) | 284 ($R_{int} = 0.060$) |
| Reflections with $I > 2\sigma(I)$ | 214 ($R_{sigma} = 0.049$) | 306 ($R_{sigma} = 0.010$) | 179 ($R_{sigma} = 0.027$) | 187 ($R_{sigma} = 0.011$) | 260 ($R_{sigma} = 0.021$) |
| Data/parameters | 215/12 | 307/12 | 202/12 | 191/12 | 284/12 |
| Goodness of fit on $F^2$ | 1.341 | 1.450 | 0.776 | 1.480 | 1.066 |
| Final $R$ indices ($I > 2\sigma(I)$) | $R1 = 0.0314$ | $R1 = 0.0169$ | $R1 = 0.0179$ | $R1 = 0.0228$ | $R1 = 0.0193$ |
| | $wR2 = 0.0752$ | $wR2 = 0.0357$ | $wR2 = 0.0356$ | $wR2 = 0.0577$ | $wR2 = 0.0435$ |
| $R$ indices (all data) | $R1 = 0.0321$ | $R1 = 0.0169$ | $R1 = 0.0226$ | $R1 = 0.0239$ | $R1 = 0.0231$ |
| | $wR2 = 0.0756$ | $wR2 = 0.0357$ | $wR2 = 0.0363$ | $wR2 = 0.0581$ | $wR2 = 0.0448$ |
| Extinction coefficient | 0.015(1) | 0.0042(4) | 0.0058(6) | 0.009(1) | 0.028(1) |
| Largest diff. peak and hole | 3.55 and $-2.39$ $e$ Å$^{-3}$ | 1.56 and $-1.18$ $e$ Å$^{-3}$ | 1.57 and $-1.18$ $e$ Å$^{-3}$ | 1.26 and $-1.42$ $e$ Å$^{-3}$ | 2.00 and $-1.96$ $e$ Å$^{-3}$ |

**Table 3.** Atomic coordinates and anisotropic displacement parameters ($pm^2$) for $RE_2Pd_2Cd$ (RE = Pr, Sm, Gd, Dy, Yb). The anisotropic displacement factor exponent takes the form $-2\pi^2[(ha^*)^2U_{11} + \cdots + 2hka^*b^*U_{12}]$. $U_{eq}$ is defined as a third of the trace of the orthogonalized $U_{ij}$ tensor. $U_{13} = U_{23} = 0$.

| Atom | Wyck. pos. | $x$ | $y$ | $z$ | $U_{11} = U_{22}$ | $U_{33}$ | $U_{12}$ | $U_{eq}$ |
|---|---|---|---|---|---|---|---|---|
| $Pr_2Pd_2Cd$ | | | | | | | | |
| Pr | 4h | 0.17416(6) | $1/2 + x$ | 1/2 | 96(4) | 108(4) | −13(2) | 100(3) |
| Pd | 4g | 0.37200(9) | $1/2 + x$ | 0 | 119(4) | 150(5) | −30(4) | 129(3) |
| Cd | 2a | 0 | 0 | 0 | 114(5) | 246(7) | 0 | 158(4) |
| $Sm_2Pd_2Cd$ | | | | | | | | |
| Sm | 4h | 0.17260(3) | $1/2 + x$ | 1/2 | 150(1) | 78(2) | −40(1) | 126(1) |
| Pd | 4g | 0.37173(5) | $1/2 + x$ | 0 | 137(2) | 137(2) | −32(2) | 137(1) |
| Cd | 2a | 0 | 0 | 0 | 106(2) | 189(3) | 0 | 134(2) |
| $Gd_2Pd_2Cd$ | | | | | | | | |
| Gd | 4h | 0.17261(4) | $1/2 + x$ | 1/2 | 68(2) | 40(2) | −20(2) | 59(2) |
| Pd | 4g | 0.37146(7) | $1/2 + x$ | 0 | 75(3) | 85(3) | −29(2) | 78(2) |
| Cd | 2a | 0 | 0 | 0 | 70(3) | 177(5) | 0 | 106(2) |
| $Dy_2Pd_2Cd$ | | | | | | | | |
| Dy | 4h | 0.17177(6) | $1/2 + x$ | 1/2 | 66(3) | 40(4) | −17(2) | 57(3) |
| Pd | 4g | 0.37093(10) | $1/2 + x$ | 0 | 67(4) | 88(6) | −26(3) | 74(3) |
| Cd | 2a | 0 | 0 | 0 | 63(5) | 152(8) | 0 | 93(4) |
| $Yb_2Pd_2Cd$ | | | | | | | | |
| Yb | 4h | 0.16850(3) | $1/2 + x$ | 1/2 | 118(1) | 119(2) | −19(1) | 118(1) |
| Pd | 4g | 0.36860(6) | $1/2 + x$ | 0 | 122(2) | 209(3) | −22(2) | 151(2) |
| Cd | 2a | 0 | 0 | 0 | 107(2) | 251(4) | 0 | 155(2) |

**Table 4.** Interatomic distances (pm) in $Gd_2Pd_2Cd$ calculated with the powder lattice parameters. Standard deviations are all equal to or smaller than 0.1 pm.

| | | | | | | | |
|---|---|---|---|---|---|---|---|
| Gd: | 2 | Pd | 286.2 | Pd: | 1 | Pd | 278.7 |
| | 4 | Pd | 299.8 | | 2 | Gd | 286.2 |
| | 4 | Cd | 340.5 | | 4 | Gd | 299.8 |
| | 1 | Gd | 374.2 | | 2 | Cd | 301.3 |
| | 2 | Gd | 376.6 | Cd: | 4 | Pd | 301.3 |
| | 4 | Gd | 401.2 | | 8 | Gd | 340.5 |

contraction, the lattice parameters decrease from the lanthanum to the lutetium compound. The crystal chemistry of the many $Mo_2FeB_2$ type compounds was reviewed recently. For further information we refer to [1] and our previous work on $Ce_2Pd_2Cd$ [3] and $Nd_2Pd_2Cd$ [7].

Finally, we comment on the ytterbium compound. Concurrent to this work, we came across the recent work on $Yb_2Pd_2Cd$ by Dhar *et al* [15]. Our data are in perfect agreement with these results. It is remarkable that $Yb_2Pd_2Cd$, besides $Yb_2Cu_2In$ [16], $Yb_2Pd_2In$ [17], and $Yb_2Au_2In$ [18, 19], is only the fourth ytterbium compound in the family of $RE_2T_2X$ intermetallics [1]. $Yb_2Cu_2In$ and $Yb_2Au_2In$ contain stable divalent ytterbium while $Yb_2Pd_2In$ and $Yb_2Pd_2Cd$ are intermediate valence systems. For $Yb_2Pd_2Cd$ signatures for heavy fermion behaviour were observed.

The course of the lattice parameters in the series of $RE_2Pd_2Cd$ compounds (table 1) shows that the $a$ parameter of $Yb_2Pd_2Cd$ fits into the series, while a strong anomaly is observed for the $c$ lattice parameter. The latter is in between the terbium and dysprosium compounds. This behaviour has been observed for several of the $RE_2T_2X$ series, e.g. comparing the

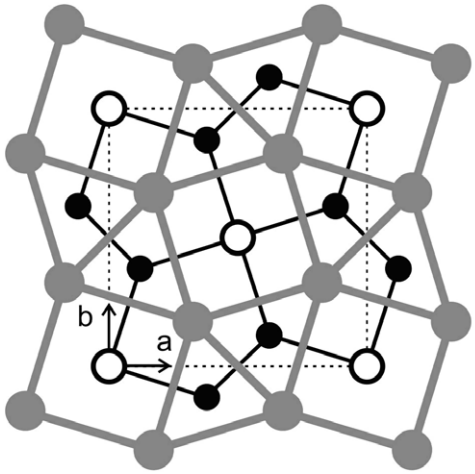


**Figure 1.** Projection of the $Gd_2Pd_2Cd$ structure onto the $xy$ plane. Gadolinium, palladium, and cadmium atoms are drawn as medium grey, filled, and open circles, respectively. All atoms lie on mirror planes at $z = 0$ (thin lines) and $z = 1/2$ (thick lines). The two-dimensional ($Pd_2Cd$) network and the distorted $AlB_2$ and CsCl related slabs are emphasized.

$RE_2Cu_2In$ and $RE_2Cu_2Mg$ compounds [20]. The $a$ parameters are mainly governed by the bonding within the $T_2X$ layers, while the $c$ parameters strongly depend on the size of the rare earth element. Similar to the positive anomaly for $Yb_2Pd_2Cd$ (tendency for larger divalent ytterbium), $Ce_2Ni_{1.88}Cd$ [4] and $Ce_2Rh_{1.86}Cd$ [6] show negative deviations for the $c$ parameters (tendency for smaller tetravalent cerium).

The $a$ lattice parameter of the $Lu_2Pd_2Cd$ sample is slightly larger than the $a$ parameter of $Tm_2Pd_2Cd$, while the $c$ parameter nicely fits into the $RE_2Pd_2Cd$ series. Similar behaviour was also observed for $Er_2Ni_2Mg$ and $Tm_2Ni_2Mg$ [21]. Most likely geometrical constraints (size of thulium and lutetium) are responsible for this behaviour. The EDX analyses gave no hint for a deviation from the ideal 2:2:1 composition and thus a homogeneity range (Lu/Mg mixing in the CsCl slab) is not the reason for this deviation.

### *3.2. Magnetic properties*

*3.2.1. $Pr_2Pd_2Cd$.* The magnetic measurement data are plotted in figures 2(a)–(d). The magnetic susceptibility ($\chi = M/H$) for $Pr_2Pd_2Cd$ measured in a field of 10 kOe is shown in figure 2(a). $Pr_2Pd_2Cd$ undergoes the paramagnetic to ferromagnetic transition at 11 K, which can be seen as a sudden upturn in the plot of $\chi$ versus $T$. The inverse susceptibility, $\chi^{-1}$ ($=H/M$) follows the Curie–Weiss law in the 100–300 K range. The paramagnetic Curie temperature, $\theta_p = 33$ K, and the effective Bohr magneton number, $\mu_{eff} = 3.51\ \mu_B$/Pr mol, were calculated from the linear region of the plot of $\chi^{-1}$ versus $T$ (in $100 < T\ (K) < 300$). The observed value of $\mu_{eff}$ is close to the expected value, 3.58 $\mu_B$ $mol^{-1}$, for a free $Pr^{3+}$ ion. The positive value of $\theta_p$ indicates the ferromagnetic interactions.

The low field susceptibility ($H = 100$ Oe) measured in the zero field cooled (ZFC) and field cooled (FC) states of the sample is shown in figure 2(b). The ZFC curve exhibits a sharp upturn at 11 K indicating the onset of ferromagnetic ordering ($T_C$) and exhibits a broad peak around 8 K. However, in the FC measurement the moment value increases as $T$ approaches 5 K, and appears to be saturating below this temperature. There is a clear ZFC–FC bifurcation around 10 K.

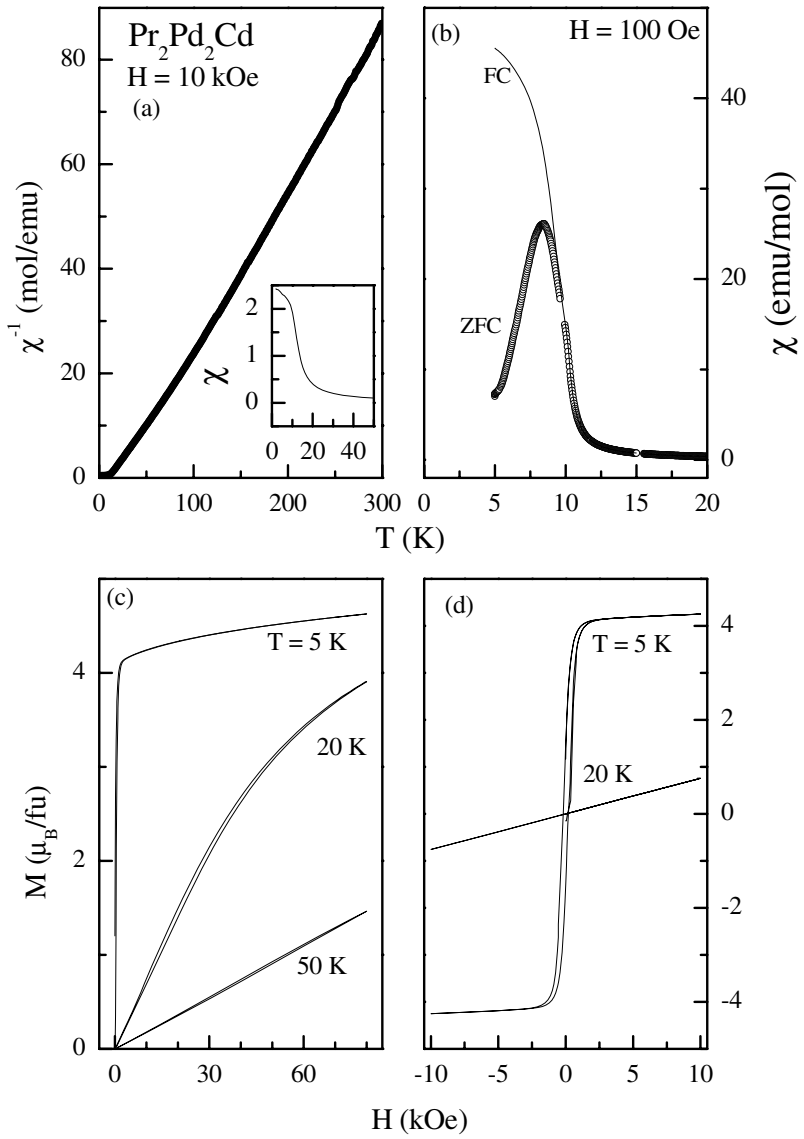


**Figure 2.** (a) Inverse susceptibility $\chi^{-1}$ for $Pr_2Pd_2Cd$ in $H = 10$ kOe (inset, $\chi$ versus $T$). (b) Low field susceptibility measured in ZFC and FC states of the sample. (c) High field magnetization at 5, 20, and 50 K. (d) Hysteresis loops measured at $T = 5$ and 20 K.

The behaviour of magnetization ($M$) as a function of field ($H$) at 5 K is consistent with the observation of ferromagnetic ordering in this compound shown in figure 2(c). $M$ increases sharply for small changes in $H$, and then increases marginally up to 80 kOe. The saturation moment value at 80 kOe/5 K is about 2.3 $\mu_B$/Pr mol, which is less than the expected value of 3.20 $\mu_B$ mol$^{-1}$ for $Pr^{3+}$. The discrepancy in the observed and expected values can be attributed to the crystal field effects. In view of the very small hysteresis, $Pr_2Pd_2Cd$ can be classified as a soft ferromagnet. There is a marked difference in the magnetism of $Pr_2Pd_2Cd$ at 5 and 20 K, particularly at high fields. The magnetic interactions persist much above the ordering temperature, which can be clearly seen by the non-linear variation of $M$ at higher fields at

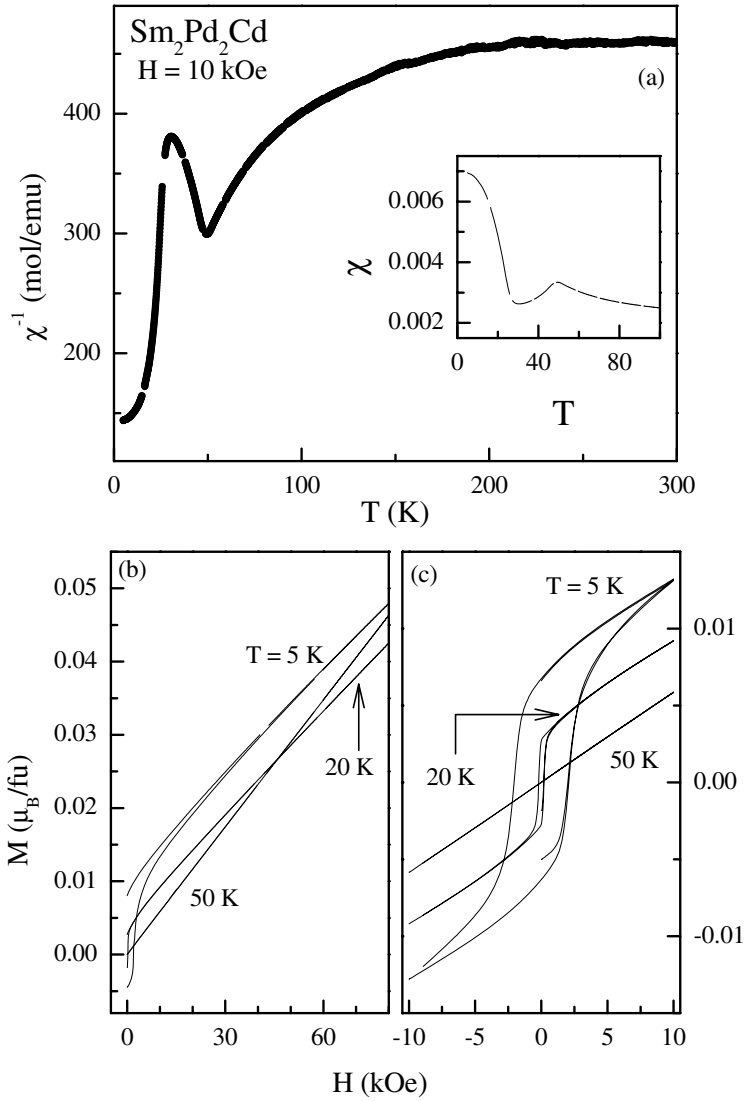


**Figure 3.** (a) Inverse susceptibility $\chi^{-1}$ for $Sm_2Pd_2Cd$ in $H = 10$ kOe. In the inset, we show $\chi$ (in units of emu mol$^{-1}$) on an expanded scale to show the features below 100 K. (b) High field magnetization at 5, 20, and 50 K. (c) Hysteresis loops measured at $T = 5$, 20, and 50 K.

20 K. The low field hysteresis behaviour measured in a field of $\pm 10$ kOe at 5 K is shown in figure 2(d). The $M(H)$ loop is hysteretic around the origin and reaches the saturation value at 250 Oe in the positive and negative directions of the applied field. The magnetism, particularly the low temperature $\chi(T)$ and $M(H)$ features of $Pr_2Pd_2Cd$, is similar to that of $Nd_2Pd_2Cd$ [7]. The hysteresis loop measured at 20 K is linear up to $\pm 10$ kOe, with no broadening of the loop around the origin.

*3.2.2. $Sm_2Pd_2Cd$.* Samarium compounds are known to exhibit interesting but complex magnetic behaviour owing to the closely placed energy levels of $Sm^{3+}$. The inverse susceptibility of $Sm_2Pd_2Cd$ measured in a field of 10 kOe is plotted in figure 3(a). $\chi^{-1}$ exhibits

van Vleck paramagnetic behaviour in the entire temperature range of the measurement. Similar magnetic behaviour was also observed for $Sm_2Pd_2Mg$ [22]. A broad peak around 50 K is observed. $\chi(T)$ however rises sharply below 25 K, implying that there is another possible magnetic transition taking place around 25 K. The sample used for the study was pure on the level of x-ray powder diffraction; however, the possibility of small paramagnetic impurities cannot be ruled out.

Continuing with unusual magnetic properties of $Sm_2Pd_2Cd$ observed in susceptibility measurements, we now look at the magnetization behaviour at temperatures $< 50$ K in figure 3(b). The $M(T)$ feature of $Sm_2Pd_2Cd$ resembles that of isostructural $Sm_2Pd_2In$ [17]; however, isotherms are prominently different, particularly at low temperatures. It should be noted that, similar to susceptibility measurements, the magnetization is negative for small fields (<2 kOe), which can be attributed to the locking of moments in the opposite direction of the field. Sometimes, as has also been observed earlier, the direction of the moment can get *locked* in the opposite direction because of small negative remanent field, and can be *unlocked* only by the application of larger fields [23].

$M(H)$ at 5 K exhibits a step in the magnetization transition around 1.2 kOe and becomes positive as $H$ approaches 2 kOe. Above 5 kOe, $M$ varies linearly with field. There is no observed step in the down cycle of $M(H)$, and it remains positive but hysteretic around the origin. This feature is more clearly seen in the $M(H)$ loop measured in a field of $\pm 10$ kOe at 5 K (figure 3(c)). There is a marked difference in $M(H)$ at 5 and 20 K as can be seen in figure 3(b). The magnetization for the initial variation of field also starts from a negative value at 20 K. A step in magnetization is seen also at 1.2 kOe and 20 K, but $M(H)$ is not hysteretic as observed at 5 K. The features of $M(H)$ at 50 K are totally different from those observed at low temperatures. $M$ increases linearly with $H$, as if the system is in the paramagnetic state.

*3.2.3. $Gd_2Pd_2Cd$.* The susceptibility $\chi$ (and $\chi^{-1}$ also, measured in a field of 10 kOe) as a function of temperature is shown in figure 4(a). $\chi^{-1}$ deviates from the Curie–Weiss behaviour below 100 K. The values of $\theta_p$ and $\mu_{eff}$ are 44.7(1) K and 8.2 $\mu_B$/Gd atom respectively. A higher moment value has been observed in several other Gd intermetallics also, and can be attributed to the polarization of the Pd 3d band with the Gd 4f moment [24].

Though there is no clear indication of an antiferromagnetic transition in $Gd_2Pd_2Cd$, the $T_N$ estimated from $d\chi/dT$ is 56 K, which makes $Gd_2Pd_2Cd$ the compound with the highest ordering temperature in the $RE_2Pd_2Cd$ series. $\chi$ increases with decreasing $T$ below $T_N$, indicating further magnetic transitions at low temperatures. Indeed, many transitions are seen in the low field ($H = 100$ Oe) susceptibility measurement shown in figure 4(b). The ZFC–FC $\chi(T)$ bifurcates around 56 K.

The magnetization curves recorded at 5 and 20 K clearly establish the antiferromagnetic nature of magnetic ordering in $Gd_2Pd_2Cd$. $M$ increases, exhibiting a curvature with increasing $H$, and at 80 kOe reaches a value of 6.5 $\mu_B$/Gd atom, which is close to the saturation moment value for a free $Gd^{3+}$ ion (given as $g_J \times J = 7$ $\mu_B$ mol$^{-1}$, for $J = 7/2$). The magnetization curves (in measurements up to 80 kOe, or hysteresis loops in $\pm 10$ kOe fields, shown in figures 4(c)–(d)) are non-hysteretic.

*3.2.4. $Tb_2Pd_2Cd$.* The susceptibility plot shown in figure 5(a) clearly shows antiferromagnetic ordering in $Tb_2Pd_2Cd$ at 55(1) K. The values of $\theta_p$ and $\mu_{eff}$ measured from the linear fit of the $\chi^{-1}$ versus $T$ plot in the 100–300 K range are 3.1(1) K and 10.0(1) $\mu_B$/Tb atom, which indicate ferromagnetic interactions and a value of $\mu_{eff}$ close to the expected free $Tb^{3+}$ moments, respectively. The ZFC–FC behaviour clearly establishes the long-range antiferromagnetic

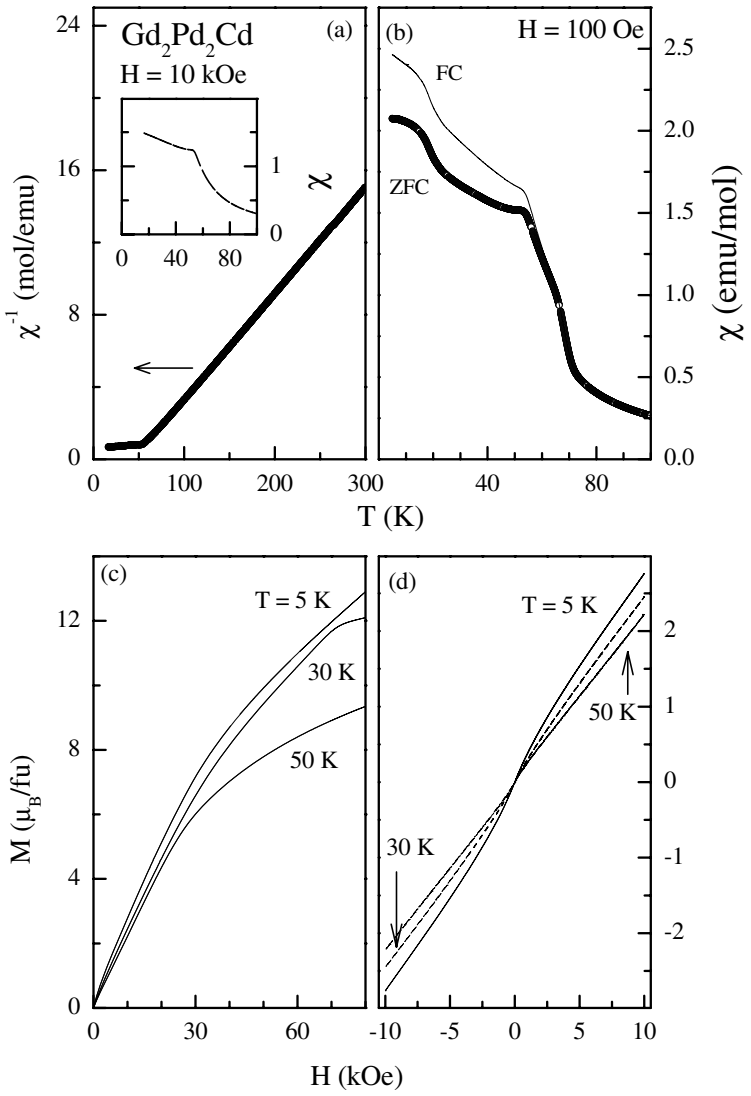


**Figure 4.** (a) Inverse susceptibility $\chi^{-1}$ for $Gd_2Pd_2Cd$ in $H = 10$ kOe (inset, $\chi$ versus $T$). (b) Low field susceptibility measured in ZFC and FC states of the sample. (c) High field magnetization at 5, 30 and 50 K. (d) Hysteresis loops measured at $T = 5$, 30 and 50 K.

ordering at 55 K. This compound also undergoes a second antiferromagnetic ordering around 25(1) K, clearly seen in the low field (100 Oe) $\chi(T)$ measurement (figure 5(b)). The bifurcation at $T < T_N$ indicates the presence of another magnetic ordering or complex nature of magnetic ordering in $Tb_2Pd_2Cd$.

The magnetization curves measured at several temperatures (after zero field cooling in each case) are shown in figure 5(c). The features at 5 K are very interesting since there are very few examples in ternary intermetallics which exhibit such a magnetization curve for a polycrystalline sample. For initial application of field, up to 20 kOe, $M$ varies linearly with $H$; as $H$ crosses this critical field the system undergoes a metamagnetic transition and there

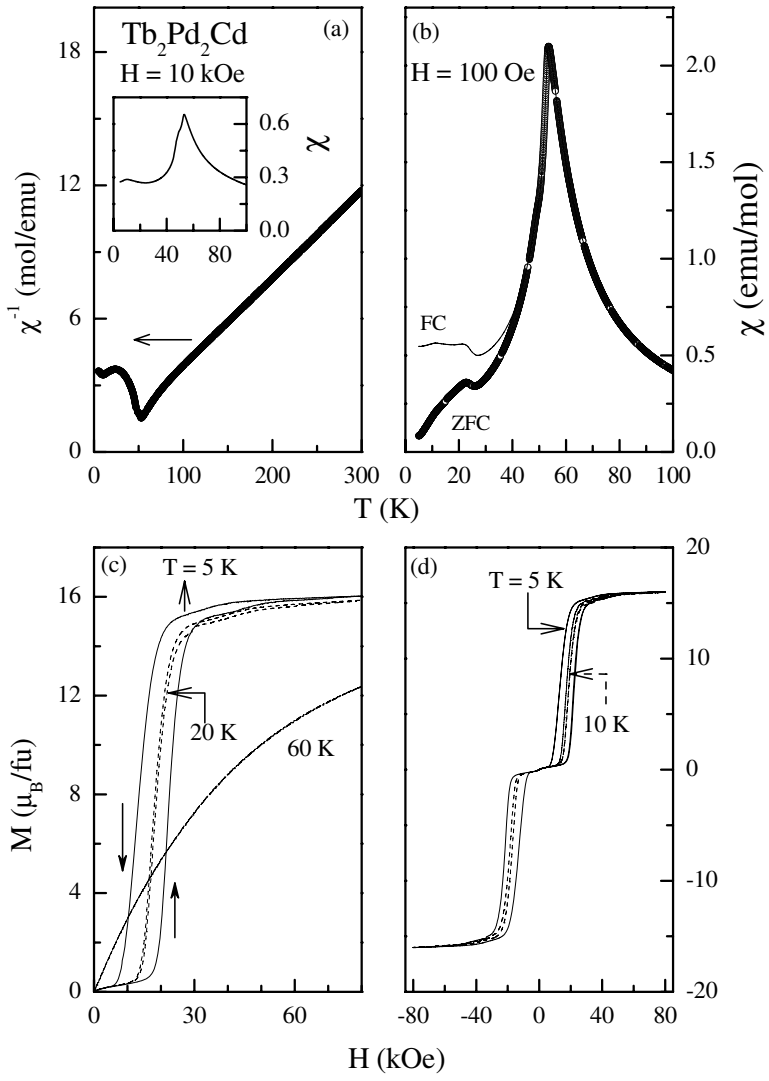


**Figure 5.** (a) Inverse susceptibility $\chi^{-1}$ for $Tb_2Pd_2Cd$ in $H = 10$ kOe (inset, $\chi$ versus $T$). The direction of the field is indicated by vertical arrows. (b) Low field susceptibility measured in the ZFC and FC states of the sample. (c) High field magnetization at 5, 20 and 60 K. (d) Hysteresis loops measured at $T = 5$ and 10 K.

is a rapid rise in $M$ for a small change in $H$. $M$ saturates to a value of about 8 $\mu_B$/Tb atom above 50 kOe, which is about 1 $\mu_B$ less than the expected value, $g \times J = 9$ $\mu_B$ mol$^{-1}$. The $M(H)$ curve in the down cycle (while reducing field to 0 Oe) is also quite interesting, as $M$ falls sharply below 20 kOe and merges with the virgin curve (up cycle curve) around 10 kOe, and then decreases linearly as field goes to 0 Oe. Another isostructural palladium containing compound exhibiting magnetization behaviour similar to that of $Tb_2Pd_2Cd$ is $Pr_2Pd_2Mg$ [22]. The pronounced square loop is seen between 10 and 20 kOe. We have also measured the hysteresis loop up to ±80 kOe at 5 K (figure 5(d)). It should also be noted here that $M(H)$ is non-hysteretic around the origin. As the temperature is increased to 20 K, the step in magnetization (spin flip transition) occurs at 15 kOe, and saturates to the previous (5 K) value

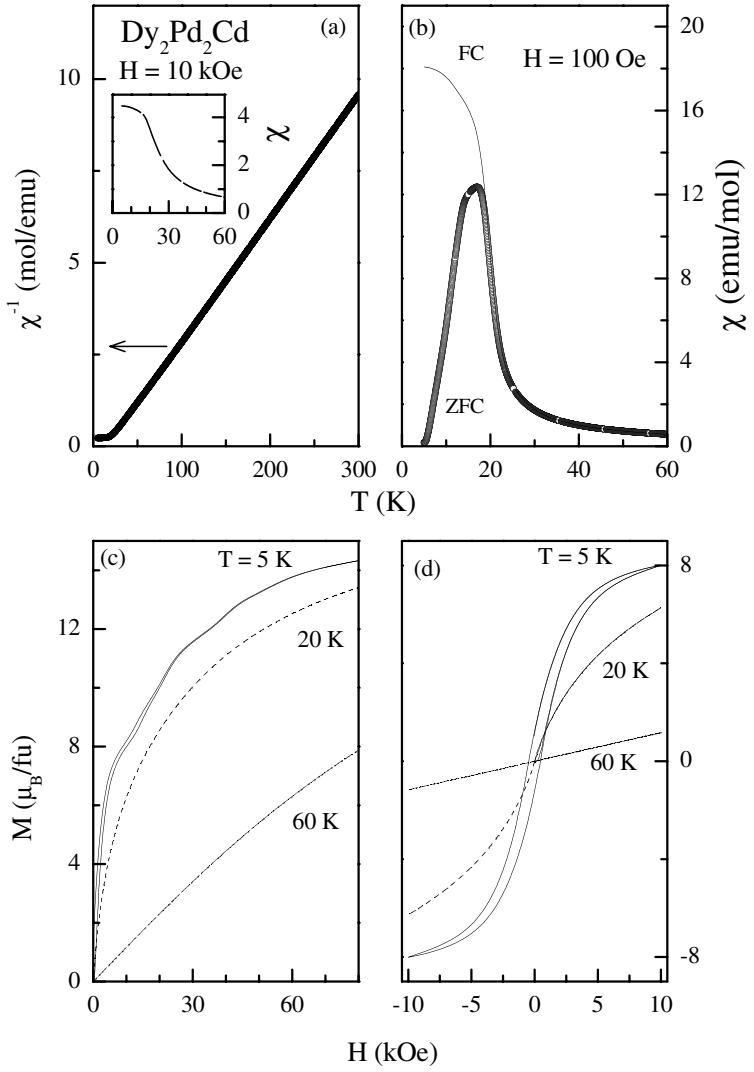


**Figure 6.** (a) Inverse susceptibility $\chi^{-1}$ for $Dy_2Pd_2Cd$ in $H = 10$ kOe (inset, $\chi$ versus $T$). (b) Low field susceptibility measured in ZFC and FC states of the sample. (c) High field magnetization at 5, 20, and 60 K. (d) Hysteresis loops measured at $T = 5$, 20, and 60 K.

of 8 $\mu_B$/Tb atom. The square loop is almost negligible here but the 5 K features are also seen at this temperature, but with different values. At 40 K the spin–flip transition also takes place, but at 10 kOe. The saturation moment reduces at 40 K, and is about 7 $\mu_B$/Tb atom. As the temperature of the measurement crosses $T_N$ (i.e. at 60 K), the spin–flip transition also vanishes and $M$ varies linearly with $H$ up to 10 kOe, above which $M$ exhibits the curvature. At 100 K ($T > T_N$) $M$ is linear up to 60 kOe.

*3.2.5. $Dy_2Pd_2Cd$.* $Dy_2Pd_2Cd$ is the third compound in the $RE_2Pd_2Cd$ exhibiting ferromagnetic ordering. $Dy_2Pd_2Cd$ undergoes the PM–FM ordering ($T_C$) at 20 K. The $\chi$ and $\chi^{-1}$ versus $T$ plots are shown in figure 6(a). $\theta_p = 17(1)$ K is close to $T_C$, and experimental $\mu_{eff} = 10.8(1)$ $\mu_B$/Dy atom is close to the expected value of 10.65 $\mu_B$ mol$^{-1}$.

In the case of low field susceptibility measurements shown in figure 6(b), the ZFC–FC increases sluggishly with a transition temperature around 20 K ($T_C$ determined from the $d\chi/dT$ curve). The increase is not as sharp as seen for the Pr compound. The ZFC exhibits a broad peak below 20 K (maximum around 18 K), with $\chi$ decreasing rapidly as $T \rightarrow 5$ K. Similar to the Pr case, the FC curve tends to saturate below 5 K. The ZFC–FC curve for the Dy compound bifurcates at 20 K. However the low temperature features of this compound are quite interesting. In the difference between the FC and ZFC curves, there is one more step around 14 K (also seen in the ZFC curve).

The magnetization measurements carried out up to the highest field of 80 kOe are shown in figure 6(c). At 5 K the curve exhibits several steps in both up and down cycles of the field ramping. Though the features are not the ones usually associated with a ferromagnetically ordered sample, the sudden rise in $M$ for small changes in $H$, and the tendency to saturate at high fields, indicates the presence of a spontaneous moment in this compound at this temperature. The small steps seen between 10 and 50 kOe can be attributed to spin-reorientation effects. The saturation moment (at 80 kOe/5 K) observed is 7.2(1) $\mu_B$/Dy atom, which is about 70% of the full saturation moment of 10 $\mu_B$ mol$^{-1}$ expected for $Dy^{3+}$. The difference in the expected and observed values can be attributed to the crystal-field effect. At 20 K, though close to the ordering temperature, $M$ increases slowly with increasing field. The hysteresis loop recorded for $Dy_2Pd_2Cd$ at 5 K is also shown in figure 6(d), which exhibits s-like shape, resembling the hysteresis curves observed in a few cluster glass compounds [25].

*3.2.6. $Er_2Pd_2Cd$.* In the entire $RE_2Pd_2Cd$ series, $Er_2Pd_2Cd$ is the only compound exhibiting two clear magnetic transitions at 12(1) and 3.6(1) K. The long-range antiferromagnetic ordering at 12(1) can be clearly seen from the plot of $\chi(T)$ in figure 7(a). $\chi$ increases sharply as $T \rightarrow 5$ K (lowest temperature in magnetic measurements), indicating another transition below this temperature. The low field $\chi(T)$ measurements in ZFC–FC states, shown in figure 7(b), establish the long range ordering (no ZFC–FC bifurcation). From the plot of $\chi^{-1}$ versus $T$ the calculated values of $\theta_p$ and $\mu_{eff}$ are 5(1) K and 9.40 $\mu_B$/Er atom. The value of $\mu_{eff}$ is close to the expected moment of 9.58 $\mu_B$ mol$^{-1}$ for $Er^{3+}$.

In $M$ versus $H$ measurement at 5 K, $Er_2Pd_2Cd$ exhibits a spin–flip transition around 10 kOe (figure 7(c)). It is also interesting to note that between 0 and 10 kOe $M$ increases non-linearly with $H$. For fields >10 kOe, $M$ increases with $H$ with a tendency to saturate above 80 kOe. The saturation moment value at 80 kOe is 6.2 $\mu_B$/Er atom, which is about 75% of the saturation moment expected for $Er^{3+}$ from $g \times J = 9.1$ $\mu_B$ mol$^{-1}$. At 20 K, much above the ordering temperatures, $M$ is linear for initial application of fields; however, for fields above 30 kOe it exhibits a curvature as it deviates from the Brillouin function, indicating that the magnetic correlations persists up to this temperature. The hysteresis loop (figure 7(d)) at 5 K shows non-linear variation of $M$ with $H$ without any appreciable anomalies around the origin (such as broadening of the loop, remanent or coercive field). At 20 K, $M$ varies linearly with field up to ±10 kOe.

### *3.3. Specific heat studies*

We now present the heat capacity behaviour of the $RE_2Pd_2Cd$ compounds, which is plotted in figure 8. The specific heat of $Pr_2Pd_2Cd$ is shown in the top panel of figure 8. The onset of the peak in $C(T)$ is around 11 K, consistent with the ordering temperature observed from the magnetic measurements. The maximum in the $C(T)$ curve is observed at 9.5(±1) K. In the same panel $C(T)$ for $Er_2Pd_2Cd$ is also shown. A well defined λ-anomaly (peak) corresponding to the long range antiferromagnetic ordering can be seen around 12(1) K for $Er_2Pd_2Cd$. A second magnetic transition at 3.6(1) K can be clearly seen here as a small peak.

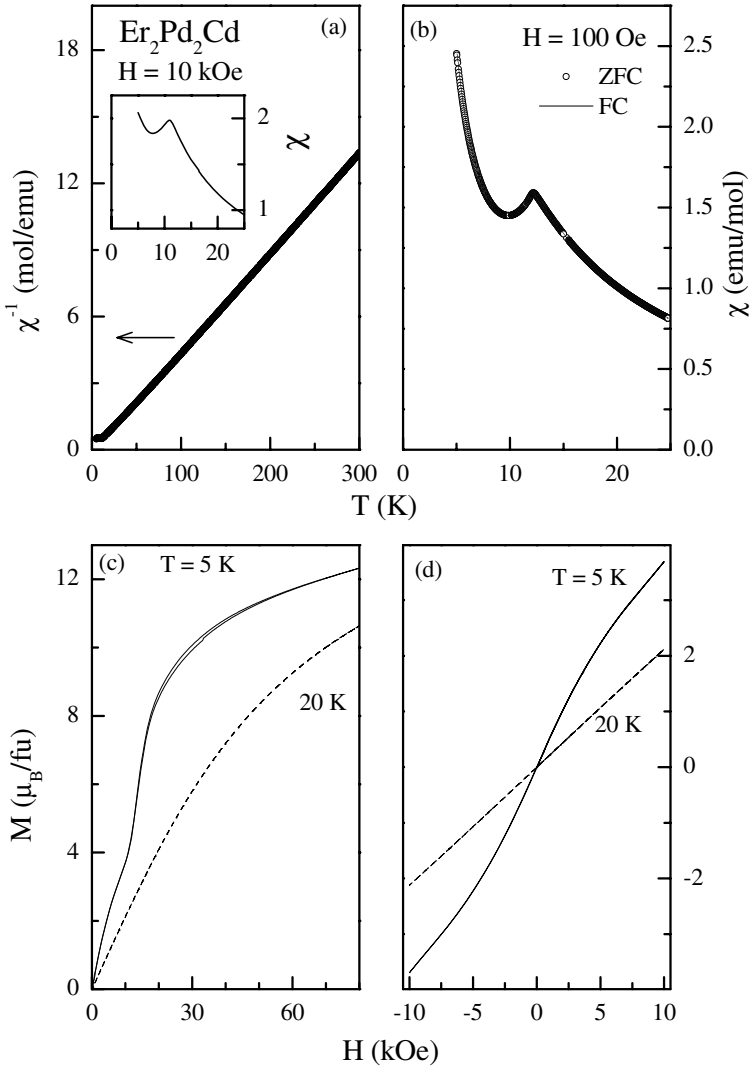


**Figure 7.** (a) Inverse susceptibility $\chi^{-1}$ for $Er_2Pd_2Cd$ in $H = 10$ kOe (inset, $\chi$ versus $T$). (b) Low field susceptibility measured in ZFC and FC states of the sample. (c) High field magnetization at 5 and 20 K. (d) Hysteresis loops measured at $T = 5$ and 20 K.

A well defined peak around 50 K is observed in $C(T)$ for $Sm_2Pd_2Cd$, which is shown in the bottom panel of figure 8. The peak around 50 K is consistent with the observations made in $\chi(T)$ measured at 10 kOe. There is no anomaly in $C(T)$ of $Sm_2Pd_2Cd$ around 25 K. The total specific heat for $Tb_2Pd_2Cd$ exhibits one peak with a λ-like anomaly at 55(1) K, in consistence with the long range antiferromagnetic ordering in this compound observed from magnetic measurements. The specific heat data ($C$ versus $T$) for $Dy_2Pd_2Cd$ exhibit a clear λ-like peak with a maximum at 18(1) K indicating the ferromagnetic ordering. A large cusp above the ordering temperature (more clearly seen in $C/T$ versus $T$), in the 30–80 K range, can be attributed to contributions from Schottky anomalies associated with heat capacity [26].

Now we turn our attention to the specific heat of $Gd_2Pd_2Cd$. In the specific heat for $Gd_2Pd_2Cd$ a well defined λ-peak associated with magnetic ordering is observed at 56(1) K.

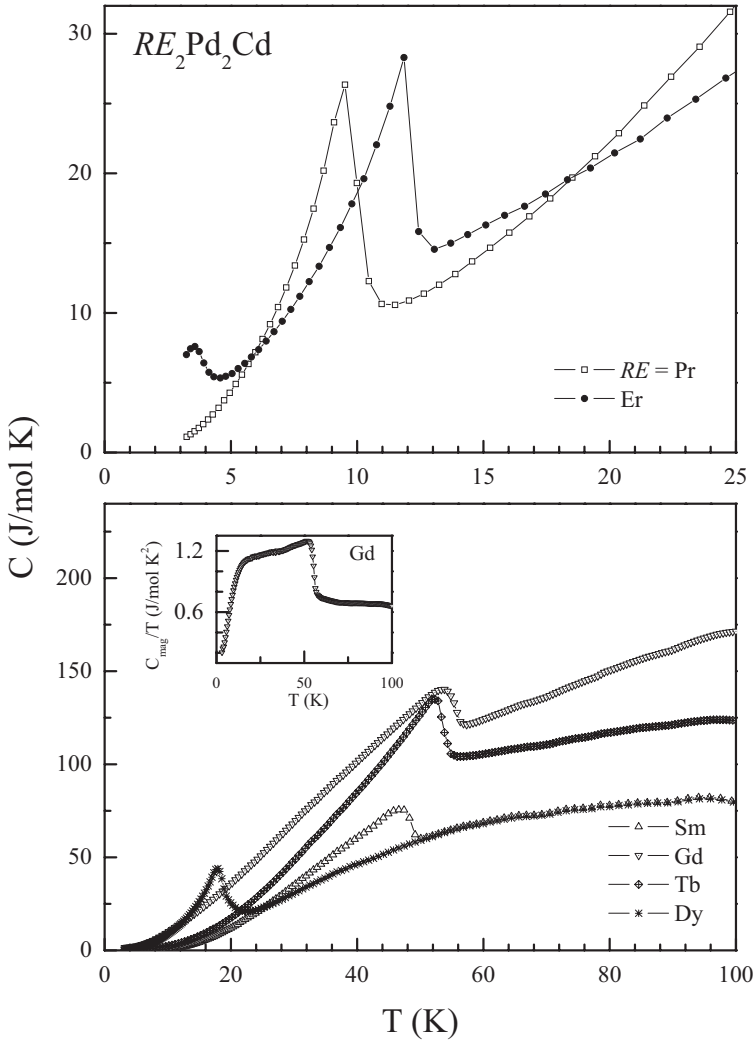


**Figure 8.** Total heat capacity ($C$) as a function of temperature ($T$) for $RE_2Pd_2Cd$ compounds. The magnetic part of heat capacity for $Gd_2Pd_2Cd$ is plotted as an inset in the bottom panel (for details see text).

Using the data of $La_2Pd_2Cd$ [7], we have estimated $C_{mag}$ for $Gd_2Pd_2Cd$ (plotted as $C_{mag}/T$ versus $T$ in the inset in the bottom panel of figure 8, using the method given by Bouvier *et al* [27]). In the linear region below 10 K in the plot of $C_{mag}/T$ versus $T^2$, the value of $\gamma$ obtained is 120(1) mJ mol$^{-1}$ K$^{-2}$. There is a flat region in the plot of $C_{mag}/T$ versus $T$ above $T_N$, indicating magnetic precursor effects. Such heavy-fermion-like behaviour has also been observed in other Gd intermetallics such as $GdCu_2Si_2$, $Gd_2PdSi_3$, $GdCuAs_2$, $GdNi_2Sn_2$, $GdPd_2In$ etc [27–32].

Another important point to observe from the plot of $C_{mag}$ versus $T$ is the jump in the value of $C_{mag}$ at $T_N$. As per the theoretical model given by Rotter *et al* [28], the jump in $C_{mag}$ around $T_N$ in an equal moment system should be around 20.1 J mol$^{-1}$ K$^{-1}$, which is indeed the case for $Gd_2Pd_2Cd$. Therefore, we propose that $Gd_2Pd_2Cd$ exhibits an equal moment magnetic structure.

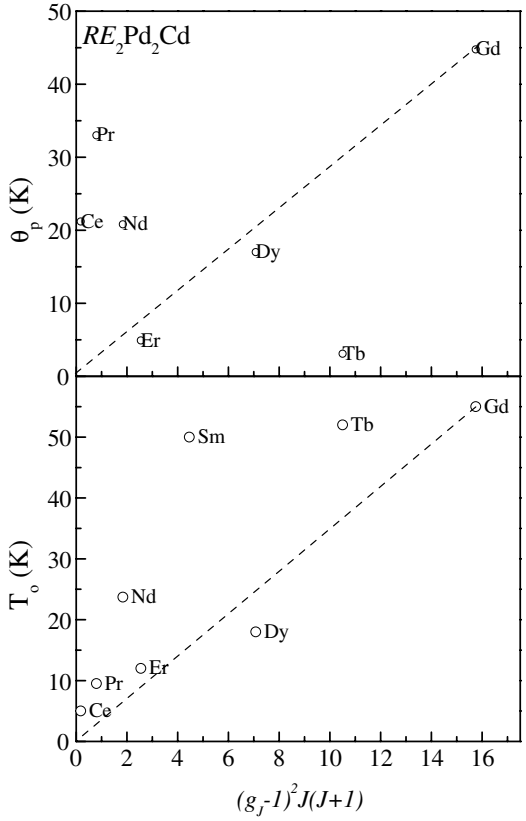


**Figure 9.** The paramagnetic Curie temperature ($\theta_p$) and the magnetic ordering temperature ($T_o$) plotted as a function of de Gennes factor, $(g_J - 1)^2 J(J + 1)$.

## 4. Conclusions

The series of isostructural $RE_2Pd_2Cd$ compounds with RE = Pr, Sm, and Gd–Lu was synthesized and structurally characterized. Various magnetic phenomena such as antiferromagnetic, ferromagnetic ordering and cluster-glass-like anomalies were observed in several of the compounds studied. The values of effective magnetic moments of the RE ions in the series of $RE_2Pd_2Cd$ compounds obtained from Curie–Weiss fits in the linear regions (in the $100 < T$ (K) $< 300$ range) of the inverse susceptibility plots are consistent with the expected magnetic moments for the free $RE^{3+}$ ions.

The magnetic properties in the $RE_2T_2X$ compounds have been predominantly governed by RKKY type interactions. Within the RKKY model, both the paramagnetic Curie temperature ($\theta_p$) and the magnetic ordering temperature ($T_o$) are expected to be proportional to the de Gennes factor, $(g_J - 1)^2 J(J + 1)$. In figures 9(a) and (b) we show the plots of $\theta_p$ and $T_o$ as a function of de Gennes factor for $RE_2Pd_2Cd$. There is a breakdown of de Gennes scaling in both cases. Several factors, such as the effect of the crystalline electric field, changes in the exchange constants and/or changes in the electron density are some of the possible reasons for the deviation from de Gennes scaling. The non-saturation of the magnetization curves at low temperatures (as low as 5 K) up to 80 kOe field in most of the compounds studied here is a further example of strong crystalline field effects at low temperatures.

The magnetization behaviour for most $RE_2Pd_2Cd$ compounds exhibits metamagnetism or complex magnetization curves (spin–flip transitions). The origin of such behaviours can be manifold, namely crystal field effect, quadrupolar interactions and/or frustration of bilinear exchange interactions etc [33]. These types of behaviours have often been found in compounds exhibiting complex magnetic phase diagrams. Therefore, we strongly believe that this work will simulate further research on these interesting compounds to understand the magnetism of ternary intermetallics exhibiting novel properties.

## Acknowledgments

We thank Dipl.-Ing. U Ch Rodewald for help with the intensity data collections. This work was supported by the Deutsche Forschungsgemeinschaft. SR is indebted to the Alexander von Humboldt Foundation for a postdoctoral stipend.

## References

[1] Lukachuk M and Pöttgen R 2003 *Z. Kristallogr.* **218** 767
[2] Emsley J 1999 *The Elements* (Oxford: Oxford University Press)
[3] Pöttgen R, Fugmann A, Hoffmann R-D, Rodewald U Ch and Niepmann D 2000 *Z. Naturf.* b **55** 155
[4] Niepmann D, Pöttgen R, Künnen B and Kotzyba G 2000 *J. Solid State Chem.* **150** 134
[5] Fickenscher Th, Rodewald U Ch, Niepmann D, Mishra R, Eschen M and Pöttgen R 2005 *Z. Naturf.* b **60** 271
[6] Stadler F, Fickenscher Th and Pöttgen R 2001 *Z. Naturf.* b **56** 1241
[7] Rayaprol S, Doğan A and Pöttgen R 2006 *J. Phys.: Condens. Matter* **18** 5473
[8] Mishra R, Pöttgen R, Hoffmann R-D, Kaczorowski D, Piotrowski H, Meyer P, Rosenhahn C and Mosel B D 2001 *Z. Anorg. Allg. Chem.* **627** 1283
[9] Rayaprol S and Pöttgen R 2005 *Phys. Rev.* B **72** 214435
[10] Rayaprol S and Pöttgen R 2006 *Phys. Rev.* B **73** 214403
[11] Pöttgen R, Gulden Th and Simon A 1999 *GIT Labor-Fachz.* **43** 133
[12] Kußmann D, Hoffmann R-D and Pöttgen R 1998 *Z. Anorg. Allg. Chem.* **624** 1727
[13] Yvon K, Jeitschko W and Parthé E 1977 *J. Appl. Crystallogr.* **10** 73
[14] Sheldrick G M 1997 *SHELXL-97, Program for Crystal Structure Refinement* University of Göttingen
[15] Dhar S K, Settai R, Ōnuki Y, Galatanu A, Haga Y, Manfrinetti P and Pani M 2007 *J. Magn. Magn. Mater.* **308** 143
[16] Tsujii N, Kitô H, Kitazawa H and Kido G 2001 *J. Alloys Compounds* **322** 74
[17] Giovannini M, Michor H, Bauer E, Hilscher G, Rogl P and Ferro R 1998 *J. Alloys Compounds* **280** 26
[18] Giovannini M, Bauer E, Michor H, Hilscher G, Galatanu A, Saccone A and Rogl P 2001 *Intermetallics* **9** 481
[19] Hulliger F 1996 *J. Alloys Compounds* **232** 160
[20] Mishra R, Hoffmann R-D and Pöttgen R 2001 *Z. Naturf.* b **56** 239
[21] Hoffmann R-D, Fugmann A, Rodewald U Ch and Pöttgen R 2000 *Z. Anorg. Allg. Chem.* **626** 1733
[22] Kraft R, Fickenscher T, Kotzyba G, Hoffmann R-D and Pöttgen R 2003 *Intermetallics* **11** 111
[23] Paulose P L, Mahesh Kumar M, Majumdar S and Sampathkumaran E V 2000 *J. Phys.: Condens. Matter* **12** 8889
[24] Sengupta K, Rayaprol S and Sampathkumaran E V 2005 *Europhys. Lett.* **69** 454
[25] Binder K and Young A P 1986 *Rev. Mod. Phys.* **58** 801
[26] Gopal E S R 1966 *Specific Heat at Low Temperatures* (New York: Plenum)
[27] Bouvier M, Lethuillier P and Schmitt D 1991 *Phys. Rev.* B **43** 13137
[28] Mallik R and Sampathkumaran E V 1998 *Phys. Rev.* B **58** 9178
[29] Rotter M, Loewenhaupt M, Döerr M, Lindbaum A and Michor H 2001 *Phys. Rev.* B **64** 014402
[30] Blanco J A, Gignoux D and Schmitt D 1991 *Phys. Rev.* B **43** 13145
[31] Sengupta K, Rayaprol S, Sampathkumaran E V, Doert Th and Jemetio J P F 2004 *Physica* B **348** 465
[32] Sampathkumaran E V, Das I, Rawat R and Majumdar S 2000 *Appl. Phys. Lett.* **77** 418
[33] Gignoux D and Schmitt D 1995 *J. Alloys Compounds* **225** 423